Design and Development of In-Process-Resolution-Tunable Stereolithography System Utilizing Two-Photon Polymerization

Makoto Shinohara, Takashi Ushida, and Katsuko S. Furukawa*

Two-photon lithography is considered a promising technology because it can achieve high resolution up to scale of 100 nm among additional processing technologies; further, it can be used to fabricate nano-/microstructures. However, it requires an unrealistic long time to obtain a practical model that is close to the human organ diameter in the order of millimeters. In this study, an in-process-resolution-tunable (iPRT) stereolithography system is reported, that realizes an optimal laser processing pathway using a new algorithm that automatically generates the processing pathway obtained by dividing the fabrication area by the effect of microstructure disappearance during the surface offset. It is demonstrated that the aforementioned algorithm can produce structures up to 50 times faster than the conventional methods and can be applied to cell culture scaffold for regenerative medicine.

1. Introduction

In additive manufacturing, the duration between design and production of a particular object is considerably low; moreover, it has wide scope for further development in the future. Multiple techniques are adopted in additive manufacturing, including sintering (selective laser sintering method)[1–4] and layered manufacturing with a binder (binder jet method).[5–7] It is widely used because 3D modeling is possible if pulverized material is available; however, since the resolution of the modeled object depends on the diameters of the powder particles, the surface morphology of the objects fabricated using 3D modeling is coarse. Additionally, the mechanical properties of the structure are subpar owing to the limited strength of the binding force among the particles. To improve the resolution and strength of a 3D modeled object, a technique of heating plastic at a temperature above its melting point and injecting it from the tip of a nozzle has been reported; however, it has a limitation that an arbitrary shape in three dimensions cannot be formed accurately.

In contrast, in stereolithography which uses a photoreactive polymer, the polymer polymerizes instantaneously, thus making it possible to freely construct a 3D shape.[8–12] Remarkable technological progress has been made in stereolithography, in terms of material properties and processing accuracy. Thus, it is one of the most promising modeling technologies at present. The stereolithography method is superior to other methods in terms of processing resolution and is suitable for processing high-performance 3D structures.

With the development of the femtosecond infrared laser, a stereolithography technique using the two-photon effect has been reported.[13–19] In this method, the two-photon polymerization (TPP) caused by the collision of two photons occurs in a narrow 3D space and, consequently 3D stereolithography is possible with an accuracy of 100 nanometers order. However, since two-photon 3D modeling has a small processing volume per unit time, the external diameter of the structure is limited to micrometer order. Therefore, the development of high-speed stereolithography technology using two-photon lasers has become highly challenging in 3D stereolithography.

In this research, we propose a new in-process resolution adjustable (iPRT) stereolithography system that can realize modeling with a high resolution and large external shape. This method uses a more efficient process by changing the solidification resolution during fabrication process and can significantly reduce the fabrication time. iPRT is an optimization method that is based on the fact that the microstructure disappears due to surface offset to divide the area that requires micromachining. Therefore, it is a technology that can be widely applied to other additive manufacturing besides two-photon lasers if the processing accuracy can be adjusted during processing. It can be a high-impact elemental technology that is expected

M. Shinohara, T. Ushida, K. S. Furukawa
Department of Mechanical Engineering
School of Engineering
The University of Tokyo
7-3-1, Hongo, Bunkyo-ku, Tokyo 113-8654, Japan
E-mail: furukawa@mech.t.u-tokyo.ac.jp

K. S. Furukawa
Department of Bioengineering
School of Engineering
The University of Tokyo
7-3-1, Hongo, Bunkyo-ku, Tokyo 113-8654, Japan

The ORCID identification number(s) for the author(s) of this article can be found under https://doi.org/10.1002/adem.202300122.

ADVANCED
SCIENCE NEWS
www.advancedsciencenews.com

ADVANCED
ENGINEERING
MATERIALS
www.aem-journal.com

to develop significantly in the future. In this study, we show that this technology can also be applied to cell culture scaffolds[20–29] for regenerative medicine.

2. Results

2.1. Laser Solidification Resolution

In laser stereolithography, an integral structure is obtained by overlapping the solidification regions for each scan to some extent with a laser. Normally, fabrication is performed with an overlap of the curing range of ≈50%, but it is necessary to know the laser solidification width to determine the absolute value of the scanning interval and to realize iPRT. First, to obtain the minimum solidification width means highest resolution, we simulated the laser power distribution to nearby focal points. The laser intensity distribution was calculated assuming the ideal TEM00 mode, and the laser diameter was hyperbolic. From the calculation results shown in **Figure 1**A, the numerical aperture (NA) of the large objective lens is ideal for accurate stereolithography, and the laser diameter should be adjusted to match NA Next, a line intersecting the strip-shaped pillar (Figure 1C) as at a right angle was fabricated, as shown in Figure 1D, and the

practical processing resolution was measured. As shown in Figure 1E, the system constructed in this study confirmed a resolution of 92 nm, which is close to the region considered the limit of the resolution of TPP. The solidification width decreased as the total laser energy irradiating the spot decreased, which is proportional to the reciprocal of the laser scanning speed and laser power (Figure 1F). It was also confirmed that the minimum solidification width is limited because curing does not occur below a certain energy threshold. Consequently, by setting an appropriate scanning interval, it is possible to obtain an integral model without the scattering of the cured product.

2.2. Fabrication Time

Next, the fabrication time was calculated. This fabrication time calculation was performed to determine the maximum processing speed of the iPRT technology. This was done by controlling the diameter of the surface shape of the object to be processed and combination of resolution of fabrication.

Three types of shapes with the same volume but different surface areas (**Figure 2**A) were processed by a new algorithm to obtain the optimum laser path. The calculation method of the optimum path using the region division by the effect of
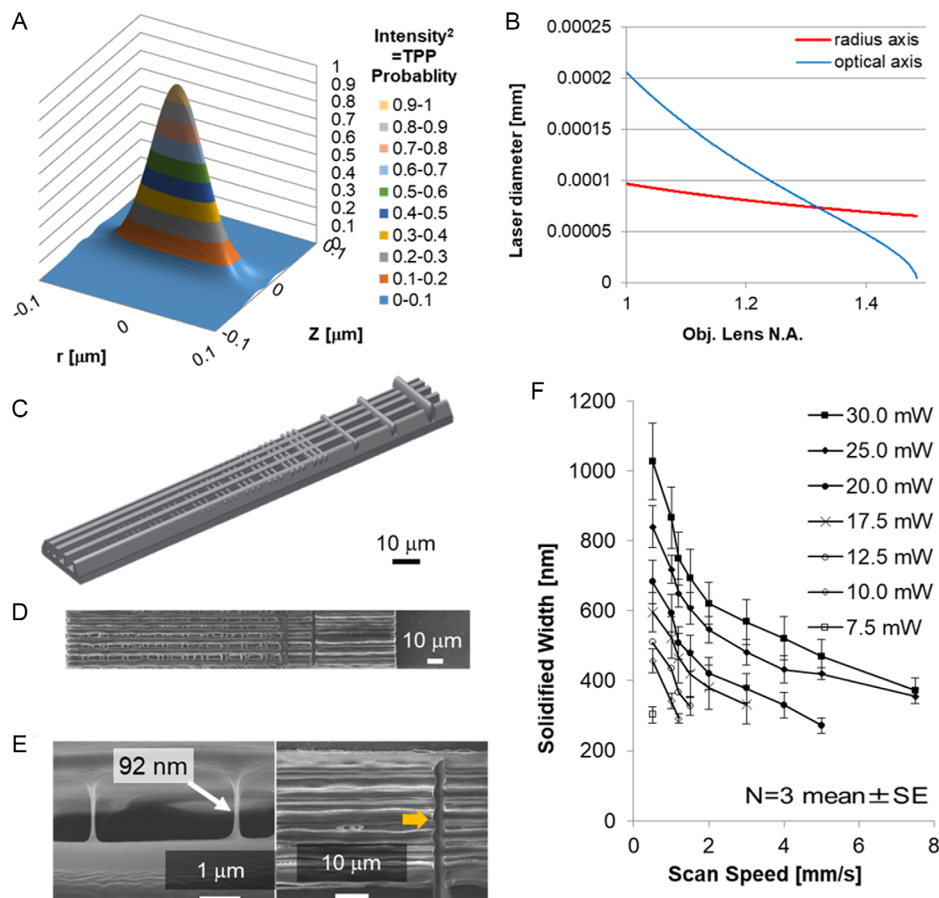

Figure 1. Fabrication resolution. A) Calculated normalized laser power distribution. Z axis is optical axis, r axis is horizontal radius axis. B) Calculated laser diameter versus objective lens NA. C) CAD design of object for resolution measurement experiment. D) Fabricated object with various line widths. E) Fabricated minimum and maximum resolution line object. F) Relationship among the scan speed, laser power, and solidified width.
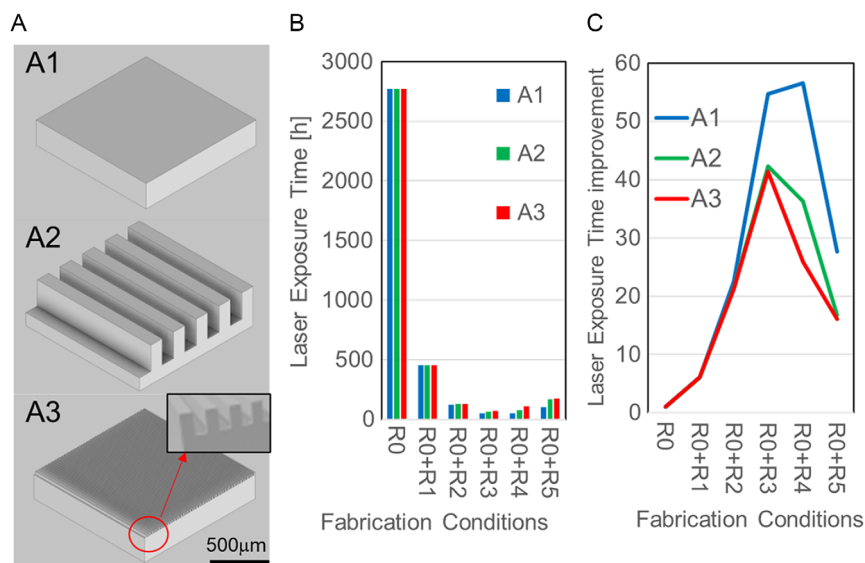
Figure 2. Fabrication time dependence on the surface structure. A) CAD design of the fabricated sample. A1: flat, A2: large pattern with width, distance, half height of 100 μm, A3: micropattern with width, distance, half height of 10 μm. R0: 100 nm of basic resolution, R1: 250 nm, R2: 500 nm, R3: 1000 nm, R4: 2000 nm, R5: 5000 nm of fast resolution. B) Calculated fabrication time. C) Improvement of fabrication time rate compared to R0 fabrication time.

disappearance of the fine structure by the surface offset is as follows. First, the shape offset inward by the distance corresponding to the high-speed modeling resolution from the surface was calculated. From there, the shape offset in reverse by the distance corresponding to the high-speed modeling resolution was calculated again. Next, it was offset inward by a distance corresponding to the fine modeling resolution. The region of the difference between this calculation result and the original shape formed the region that needed to be microfabricated. Each area was sliced at each resolution interval, scanned, and filled, and the modeling time was calculated from the total length.

Three types of cross-sectional views of the object shape with same volume were prepared: a simple rectangle and a shape with a rectangular surface pattern of two width scales of 100 and 10 μm, named, A1, A2, and A3, respectively. The width was set to be the same size, and the height was set to be twice the size of the width. As a result, shapes with the same volume but different surface areas will be processed.

The fabrication conditions were a combination of a fine modeling resolution of 100 nm called R0 and a high-speed modeling resolution (R1–R5). The fabrication conditions are shown in **Table 1**. The high-speed modeling resolution combined by the iPRT method was selected from one of the lengths of 250, 500, 1000, 2000, and 5000 nm called R1, R2, R3, R4, and R5, respectively. Figure 2B and Table 1 show the results of the fabrication time calculation, and Figure 2C and **Table 2** show the results of the improvement rate calculation. Utilizing iPRT, high-speed machining of R0 + R3 and R0 + R4 was confirmed to be 50 times faster than conventional monoresolution method. Thus, the larger the combined resolution, the shorter the fabrication time (R0 + R1–3); however, if the combined resolution becomes too large, the fabrication time becomes longer (R0 + R4, 5). Optimal combination resolution is associated with surface structural dimensions. The larger the surface area and

Table 1. Calculated fabrication time and measurement conditions.

Fabrication resolution[a]	A1 fabrication time [h]	A2 fabrication time [h]	A3 fabrication time [h]
R0: 100 nm	2774	2773	2773
R0 + R1: 250 nm	452	456	457
R0 + R2: 500 nm	122	130	130
R0 + R3: 1,000 nm	51	66	67
R0 + R4: 2,000 nm	49	76	107
R0 + R5: 5,000 nm	100	165	172

[a]A1, A2, A3: objects which have different surface areas with the same volume. A1: simple rectangular, A2: rectangular with 100 mm scale pattern, A3: rectangular with 10-mm scale pattern. R0, R1, R2, R3, R4, R5: conditions with the resolution of 100, 150, 500, 1000, 2000, 5000 nm.

Table 2. Fabrication time improvement ratio.

Fabrication resolution[a]	A1 ratio[b]	A2 ratio	A3 ratio
R0: 100 nm	1.00	1.00	1.00
R0 + R1: 250 nm	6.14	6.08	6.07
R0 + R2: 500 nm	22.7	21.4	21.3
R0 + R3: 1,000 nm	54.8	42.3	41.4
R0 + R4: 2,000 nm	56.6	36.3	26.0
R0 + R5: 5,000 nm	27.6	16.8	16.1

[a]The ratios were calculated by dividing the time required for the designated combinations by the time required for R0; [b]A1, A2, A3: objects which have different surface areas with the same volume. A1: simple rectangular, A2: rectangular with 100 mm scale pattern, A3: rectangular with 10-mm scale pattern. R0, R1, R2, R3, R4, R5: conditions with resolution of 100, 150, 500, 1000, 2000, 5000 nm.

**ADVANCED
SCIENCE NEWS**

www.advancedsciencenews.com

**ADVANCED
ENGINEERING
MATERIALS**

www.aem-journal.com

the more complex the structure, the slower the rate of improvement. For optimum fabrication, it is necessary to match the fabrication conditions to the diameter of the surface structure. Otherwise, the fabrication time will be long.

2.3. 3D Free Fabrication

Finally, to demonstrate the effectiveness of the iPRT system, we fabricated 3D structures. **Figure 3**A depicts cross-sectional views of the laser scanning path when iPRT is not used (conventional modeling method) and when iPRT is used, and the white dots indicate the coordinates for scanning. The combined processing conditions were 100 nm and 1000 nm. By offsetting the surface shape as described above, the surface volume required for high accuracy was extracted. The left side of Figure 3A shows that the path is dense because the solidification diameter is small, and the right side shows that the internal scanning is sparse and only the surface treatment is dense. Figure 3B shows the processed object. By optimizing the laser path and resolution, smooth and hollow structures can be created quickly. In addition, as shown in Figure 3C, we fabricated a structure that is hollow and has a pathway for cells to invade and supply nutrients and that can be used as a scaffold for cell culture used in regenerative medicine. Additionally, a micropattern is shown in Figure 3D for cell differentiation. Therefore, it was confirmed that iPRT can produce micro-/nanoscale objects at high speed and with high accuracy.

3. Discussion

In this research, iPRT stereolithography system was developed that realizes optimum processing by changing each processed part divided by region division because of microstructure disappearance due to surface offset to the optimum processing resolution during processing. Using this system, high-speed stereolithography using a two-photon laser was realized. Since this technology can contribute to high-speed modeling of any object regardless of its shape, it can play a vital role in the advancement of 3D modeling.

iPRT is a method for performing optimum machining on the result of region division, and it does not depend on the wave characteristics of the laser. It can also be applied to other 3D printing methods, such as fused deposition modeling (FDM), binder jet method (BJM), and selective laser sintering (SLS) method, by changing the machining volume per unit time as well as controlling the curing range by the laser.

The iPRT method can also be applied to manufacturing in various fields. As an example, we demonstrated that hollow scaffold used for 3D regeneration culture of organs is highly useful in regenerative medicine and that it can be processed using this system.

The current TPP method is limited to nano–micrometer microfabrication and cannot be extended to the millimeter scale. For example, it requires 10^2 order of fabrication time to produce a 1 mm × 1 mm × 1 mm object with a resolution of 100 nm and
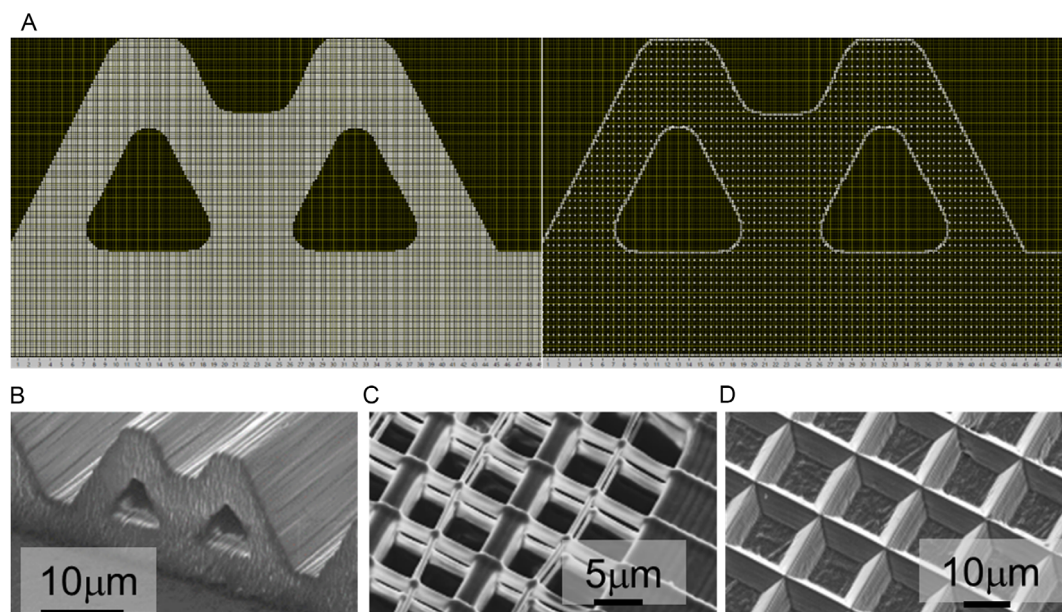

Figure 3. Fabricated 3D structure. A) Optimization of cross section of the laser pathway for the 3D structure with an overhang. Left: only precise method, dense white dots can be seen like white mesh. Right: with iPRT method, only the surface is dense and can be seen as a white line, inner part looks gray because of sparse white dots. B) Fabricated 3D structure with an overhang based on iPRT. C) Fabricated cell culture scaffold-like hollow structure. Thick line fabricated at 1 µm, thin line fabricated at 100 nm. The external frame and the thick vertical grid were fabricated by arranging thick lines, and the horizontal grid with medium thickness was fabricated with a single thick line. The thin vertical lines were fabricated with a single thin line. This 3D lattice was fabricated by stacking such structures. D) Fabricated triangular micropattern. Thick line fabricated at 1 µm; thin line fabricated at 100 nm. By designing a structure with a triangular cross section, by drawing thick lines in the center and thin lines on the surface, arranging them periodically and scanning them in both the X and Y directions, triangular lattice micropattern was fabricated.

a porosity of 90%. Therefore, it is necessary to increase the speed by the order of 10^2 or higher while maintaining the processing accuracy.

There are two main methods for high-speed machining, one is to increase the number of focal points or expand exposed area and the other is to increase the scanning speed; however, the results from both the methods are limited. As a method of increasing the number of focal points, 3× speed improvements are reported using holograms;[30,31] however, this limits the resolution of the method. 3× speed[32–34] for plane construction by digital mirror device (DMD) is limited to simple pattern creation, and like hologram, it requires an expensive and complicated setup. A method to expand the exposed area is reported using light sheet,[35] however, this method cannot be used with TPP. Using a micromirror array to increase the processing speed is over ten times faster.[36] In addition, if a galvanometer is used, the speed will be ten times faster,[37] but to process at a 10^2 times higher speed, a powerful 10 W class laser that is ten times more expensive is required.

The iPRT method has the advantage of freely processing precise objects without the need for complicated setups or powerful lasers. Currently, iPRT can process up to 50 times faster than conventional methods. Increasing the intensity of the laser increases the processing volume per unit time by about to the third power, but the increasing the scanning speed works only by to the first power; thus, a particularly strong laser is not required.

Meanwhile, since iPRT is an area division method, it can be combined with a Galvano scan method or a surface drawing method such as DMD or hologram. However, this can be costly as it requires a complex setup and a more powerful laser.

It was demonstrated that iPRT can create a cell culture scaffold with a hollow structure for regenerative medicine. In addition, we have developed a highly expandable and versatile technology that can be applied not only to regenerative medicine but also to the fields of energy and photonics because it can produce fine structures on a large scale.

4. Conclusion

In this study, we developed an iPRT stereolithography device that demonstrates nanoscale precision and high-speed fabrication. Compared with conventional methods, up to 50 times higher fabrication speed can be achieved using our device.
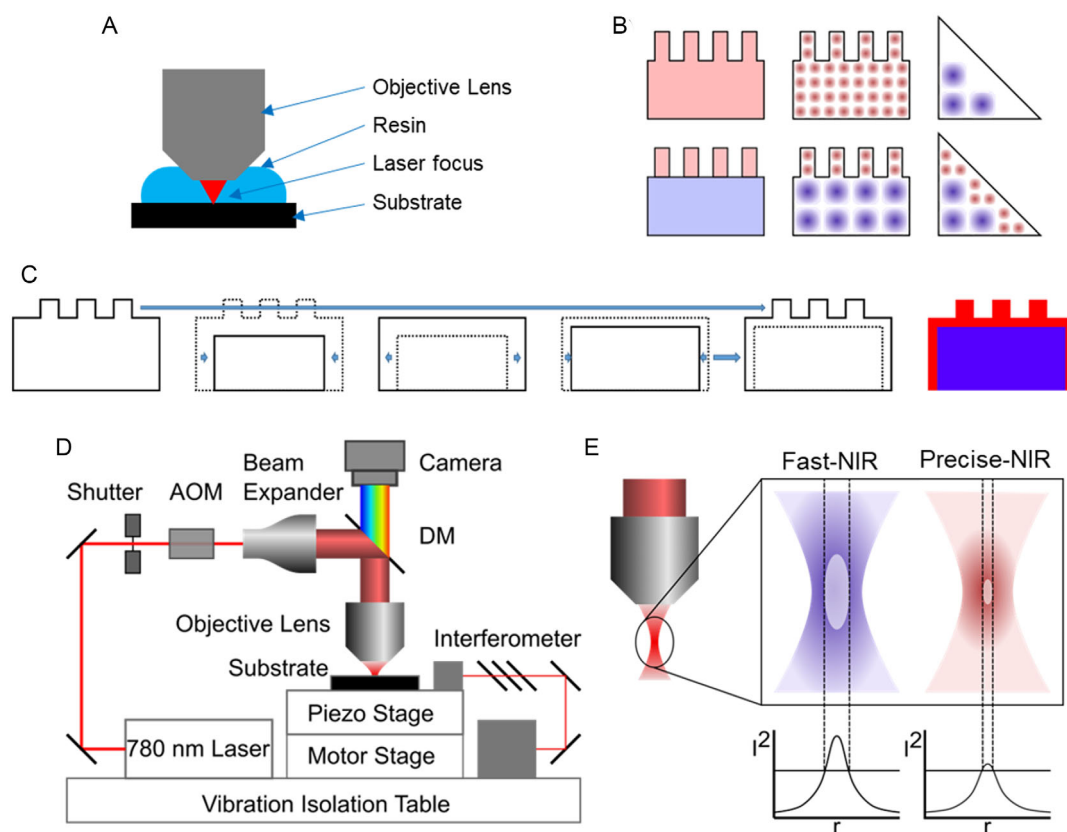

Figure 4. Fabrication system setup. A) Objective lens and resin setup. This system adopted the dip-in setup. Dip-in method has the advantages of flexibility of movement and longer working distance filled with high-refractive-index resin, thus resulting in high resolution. B) Hybrid drawing method. High-resolution drawing results in longer processing time; low resolution results in rough surfaces. With hybrid drawing, processing time is reduced with a smooth surface. C) SOE. When offset is implemented, small structures disappear. With reverse offset, small structure areas can be obtained. With comparison between pre- and postoffset shape, small structure areas can be obtained. D) Schematic of iPRT stereolithography. Femtosecond laser is controlled by a shutter and acoustic optic module (AOM), expanded with a beam expander, and focused with a high-NA objective lens. Motor and piezostages are merged with an interferometer. E) NIR two-photon fabrication resolution tunability.

2300122 (5 of 7)

Objects were freely designed with computer-aided design (CAD), and its applicability with biocompatible materials was also confirmed.

We demonstrated the feasibility of producing scaffolds with transplantable dimensions by iPRT's high-speed fabrication. The system and algorithm can be applied to further develop 3D printing technologies.

5. Experimental Section

Optimization Principle: The ability to adjust the resolution midfabrication to optimize the structure is unique to our iPRT system. Specifically, the inner support was solidified using the high-speed fabrication method, followed by a precision method to solidify the surface topography (**Figure 4**A). With the combined technique, the fabrication time can be reduced compared to using the precision method only. Geometry data were designed in CAD software, converted to STL, sliced with a proprietary software, and converted to voxel data. This data was then divided into micromachining and high-speed machining areas using the surface offset effect (SOE). If the surface offset distance was larger than the microstructures' diameters, structures will disappear through the surface offset process. Comparing the original data and post-offset data, data area of microstructures can be obtained, as shown in Figure 4B. Scanning parameters were selected manually, but once selected, scan path dimensions were computed automatically, and the data was exported for the laser to scan each area with appropriate distances.

Experimental Setup: Our stereolithography system utilized the dip-in system (Figure 4A), which directly dipped the objective lens to a photosensitive resin. Silicon wafers were coated with Ormoprime (Microresist Technologies) to promote adhesion of the solidified resin on the substrate. Motion stages were combined with precise piezostages and a long-range linear motor stage to achieve long stroke and accuracy. Their absolute position was measured by external interferometer and laser was switched based on the position information. The axes of the stages were also adjusted using a proprietary software.

Laser and Optics: 100 mW NIR and 10-femtosecond class laser (Femtolasers Integral Pro100) was used as the ultrashort pulse laser for TPP for our iPRT system; a schematic view is shown in Figure 4D. TPP can polymerize resin with higher precision compared to conventional SPP (Figure 4E). The laser was modulated via Acoustic Optic Module (AOM) (ISOMET). The beam diameter was optimized for the objectives using a beam expander (Edmund Optics). NIR reflective and visible light transmitting dichroic mirrors (Sigma Koki) were placed in front of the objective lens to guide and focus the visible light into the camera. 100× N. A. 1.45 lens (Carl Zeiss) was selected as the objective lens due to its high N.A values, resulting in high resolution.

Resin: Photosensitive resin (Ormocomp, MicroResist Technologies) was used for the microfabrication of 3D cell culture scaffolds owing to its biocompatibility[9,10] and compatibility as a mold for producing PDMS scaffolds via soft lithography. The resin was cured into the desired structure on the silicon wafer, rinsed with OrmoDEV (MicroResist Technologies), and then postcured under UV light for 2 min.

Conflict of Interest

The authors declare no conflict of interest.

Data Availability Statement

Research data are not shared.

[1] S. F. S. Shirazi, S. Gharehkhani, M. Mehrali, H. Yarmand, H. S. C. M. Metselaar, N. A. K. Kadri, N. A. A. Osman, *Sci. Technol. Adv. Mater.* **2015**, *16*, 033502.

[2] J. N. DiNoro, N. C. Paxton, J. Skewes, Z. Yue, P. M. Lewis, *Polymers* **2022**, *9*, 2336.

[3] E. Tikhomirov, M. Åhlén, N. D. Gallo, M. Strømme, T. Kipping, J. Quodbach, J. Lindh, *Int. J. Pharm.* **2023**, *635*, 122780.

[4] D. Oropeza, A. J. Hart, *Int. J. Adv. Manuf. Technol.* **2021**, *114*, 3459.

[5] C. L. Cramer, P. Nandwana, J. Y. S. F. Evans, A. M. Elliott, C. Chinnasamy, M. P. Paranthaman, *Heliyon* **2019**, *5*, 02804.

[6] K. Sen, A. Manchanda, T. Mehta, A. W. K. Ma, B. Chaudhuri, *Int. J. Pharm.* **2020**, *30*, 119430.

[7] A. Mostafaei, Y. Behnamian, Y. L. Krimer, E. L. Stevens, J. L. Luo, M. Chmielus, *Data Brief* **2016**, *9*, 556.

[8] K. Peng, X. Liu, H. Zhao, H. Lu, F. Lv, L. Liu, Y. Huang, S. Wang, Q. Gu, *ACS. Appl. Bio. Mater.* **2021**, *17*, 4549.

[9] P. E. Petrochenko, J. Torgersen, P. Gruber, L. A. Hicks, J. Zheng, G. Kumar, R. J. Narayan, P. L. Goering, R. Liska, J. Stampfl, A. Ovsianikov, *Adv. Healthcare Mater.* **2015**, *2*, 739.

[10] R. F. Pereira, P. J. Bártolo, *Engineering* **2015**, *1*, 90.

[11] H. Kadry, S. Wadnap, C. Xu, F. Ahsan, *Eur. J. Pharm. Sci.* **2019**, *1*, 60.

[12] E. R. Rossegger, J. Strasser, R. Höller, M. Fleisch, M. Berer, S. Schlögl, *Macromol. Rapid Commun.* **2023**, *44*, e2200586.

[13] A. M. Kasko, D. Y. Wong, *Future Med. Chem.* **2010**, *2*, 1669.

[14] A. Ovsianikov, S. Schlie, A. Ngezahayo, A. Haverich, B. N. Chichkov, *J. Tissue Eng. Regen. Med.* **2007**, *1*, 443.

[15] S. Kawata, H. B. Sun, T. Tanaka, K. Takada, *Nature* **2001**, *412*, 697.

[16] D. Wu, Q. D. Chen, L. G. Niu, J. N. Wang, J. Wang, R. Wang, H. Xia, H. B. Sun, *Lab Chip* **2009**, *9*, 2391.

[17] T. Weiß, G. Hildebrand, R. Schade, K. Liefeith, *Eng. Life Sci.* **2009**, *9*, 384.

[18] C. N. LaFratta, J. T. Fourkas, T. Baldacchini, R. A. Farrer, *Angew. Chem. Int. Ed.* **2007**, *46*, 6238.

[19] H. Takahashi, S. Hasegawa, A. Takita, Y. Hayasaki, *Opt. Express* **2008**, *16*, 16592.

[20] W. R. Kim, M. J. Jang, S. Joo, W. Sun, Y. Nam, *Lab Chip* **2014**, *14*, 799.

[21] C. H. Seo, K. S. Furukawa, K. Montagne, H. Jeong, T. Ushida, *Biomaterials* **2011**, *32*, 9568.

[22] C. Zhao, X. Wang, L. Gao, L. Jing, Q. Zhou, J. Chang, *Acta Biomater.* **2018**, *73*, 509.

[23] D. A. Kidwell, W. K. Lee, K. Perkins, K. M. Gilpin, T. J. O'Shaughnessy, J. T. Robinson, P. E. Sheehan, S. P. Mulvaney, *ACS. Appl. Mater. Interfaces* **2019**, *11*, 19793.

[24] K. Obata, J. Koch, U. Hinze, B. N. Chichkov, *Opt. Express* **2010**, *18*, 17193.

[25] A. P. Zhang, X. Qu, P. Soman, K. C. Hribar, J. W. Lee, S. Chen, S. He, *Adv. Mater.* **2012**, *24*, 4266.

**ADVANCED
SCIENCE NEWS**

www.advancedsciencenews.com

**ADVANCED
ENGINEERING
MATERIALS**

www.aem-journal.com

[26] C. H. Seo, K. S. Furukawa, Y. Suzuki, N. Kasagi, T. Ichiki, T. Ushida, *Macromol. Biosci.* **2011**, *11*, 938.

[27] C. H. Seo, H. Jeong, K. S. Furukawa, Y. Suzuki, T. Ushida, *Biomaterials* **2013**, *34*, 1764.

[28] C. H. Seo, H. Jeong, Y. Feng, K. Montagne, T. Ushida, Y. Suzuki, K. S. Furukawa, *Biomaterials* **2014**, *35*, 2245.

[29] H. Jeong, X. Yang, Z. Pei, T. Ushida, K. S. Furukawa, *J. Biomech. Sci. Eng.* **2020**, *15*, 20-00009.

[30] L. Yang, A. El-Tamer, U. Hinze, J. Li, Y. Hu, W. Huang, J. Chu, B. N. Chichkov, *Opt. Lasers Eng.* **2015**, *70*, 26.

[31] W. D. Mao, G. Q. Liang, Y. Y. Pu, H. Z. Wang, Z. Zeng, *Appl. Phys. Lett.* **2007**, *91*, 261101.

[32] Y. Kim, A. D. Maxwell, T. L. Hall, Z. Xu, K. W. Lin, C. A. Cain, *IEEE Trans. Ultrason. Ferroelectr. Freq. Control* **2014**, *61*, 1559.

[33] Q. Geng, D. Wang, P. Chen, S. C. Chen, *Nat. Commun.* **2019**, *10*, 2179.

[34] E. J. Mott, M. Busso, X. Luo, C. Dolder, M. O. Wang, J. P. Fisher, D. Dean, *Mater. Sci. Eng. C* **2016**, *61*, 301.

[35] A. Madrid-Sánchez, F. Duerr, F. Duerr, Y. Nie, Y. Nie, H. Thienpont, H. Thienpont, H. Ottevaere, H. Ottevaere, *Int. J. Bioprint.* **2022**, *9*, 650.

[36] S. K. Saha, D. Wang, V. H. Nguyen, Y. Chang, J. S. Oakdale, S. C. Chen, *Science* **2019**, *366*, 105.

[37] K.-C. Cho, C.-H. Lien, C.-Y. Lin, C.-Y. Chang, L. L. H. Huang, P. J. Campagnola, C. Y. Dong, S.-J. Chen, *Opt. Express* **2011**, *19*, 11732.

2300122 (7 of 7)